

Enzyme-Directed Assembly of Nanoparticles in Tumors Monitored by *in Vivo* Whole Animal Imaging and *ex Vivo* Super-Resolution Fluorescence Imaging

Miao-Ping Chien,[†] Andrea S. Carlini,[†] Dehong Hu,[§] Christopher V. Barback,[‡] Anthony M. Rush,[†] David J. Hall,[‡] Galya Orr,[§] and Nathan C. Gianneschi^{*,†}

[†]Department of Chemistry and Biochemistry and [‡]Department of Radiology, University of California, San Diego, La Jolla, California 92093, United States

[§]Environmental Molecular Sciences Laboratory, Pacific Northwest National Laboratory, Richland, Washington 99354, United States

S Supporting Information

ABSTRACT: Matrix metalloproteinase enzymes, overexpressed in HT-1080 human fibrocarcinoma tumors, were used to guide the accumulation and retention of an enzyme-responsive nanoparticle in a xenograft mouse model. The nanoparticles were prepared as micelles from amphiphilic block copolymers bearing a simple hydrophobic block and a hydrophilic peptide brush. The polymers were end-labeled with Alexa Fluor 647 dyes leading to the formation of labeled micelles upon dialysis of the polymers from DMSO/DMF to aqueous buffer. This dye-labeling strategy allowed the presence of the retained material to be visualized via whole animal imaging *in vivo* and in *ex vivo* organ analysis following intratumoral injection into HT-1080 xenograft tumors. We propose that the material is retained by virtue of an enzyme-induced accumulation process whereby particles change morphology from 20 nm spherical micelles to micrometer-scale aggregates, kinetically trapping them within the tumor. This hypothesis is tested here via an unprecedented super-resolution fluorescence analysis of *ex vivo* tissue slices confirming a particle size increase occurs concomitantly with extended retention of responsive particles compared to unresponsive controls.

In this paper we demonstrate enzyme-driven retention of a polymeric microscale scaffold within tumor tissue via the injection of nanoscale, matrix metalloproteinase-responsive micellar nanoparticles.^{1–12} In recent work from our laboratory,¹ we described the first example of an enzyme-programmed tissue-targeted nanoparticle probe and utilized a Förster resonance energy transfer (FRET) based assay for monitoring particle accumulation.^{1,13,14} Generation of a FRET signal provided evidence that the nanoparticles had undergone an enzyme-directed aggregation process in tumor tissue generating a slow clearing, self-assembled “implant” of polymeric material within the tissue.¹ Based on those results, we hypothesized that the materials had passively diffused into the tumors following injection and then undergone a size increase, which trapped the material within the extracellular space within the tissue. To test this hypothesis, we synthesized a new set of polymeric micellar nanoparticles, prepared from the self-assembly of amphiphilic block copolymers consisting of a hydrophilic peptide brush

generated via graft-through polymerization of peptide-based monomers^{15,16} and a simple hydrophobic block (Figure 1). We term these synthons for generating enzyme-responsive nanoparticles, peptide-polymer amphiphiles (PPAs). The PPAs in this study were labeled with Alex Fluor 647 to generate micelles labeled on their periphery with multiple dye molecules. This dye was chosen for two key reasons: (1) it is known that whole mouse imaging is facilitated by the long excitation and emission wavelength of the fluorophore ($\lambda_{\text{ex}} = 635 \text{ nm}$, $\lambda_{\text{em}} = 670 \text{ nm}$, in this study), and (2) this photoswitching dye is amenable to analysis via super-resolution fluorescence microscopy by employing stochastic optical reconstruction microscopy (STORM).^{17–19} The emergence of super-resolution fluorescence microscopy techniques^{18,20,21} has allowed researchers to overcome the diffraction limit and enables the examination of various processes occurring at the submicrometer scale.^{22–24} Surprisingly, nanomaterials used in the delivery of therapeutics and diagnostics are rarely characterized via these useful super-resolution techniques,^{25–27} in particular in cellular *in vitro* or in *ex vivo* tissue analysis studies. However, despite this lack of precedence, we determined that such an approach would be needed to confirm whether nanoscale particle accumulation into larger aggregates was occurring within the tumor tissue postinjection.

Two micelles, **M** and **M_D** were prepared from two different PPAs (Figures 1 and 1S). **M** was generated from a PPA consisting of a peptide prepared with L-amino acids as an active substrate for matrix metalloproteinases (MMPs), known to be overexpressed in certain tumor tissues.^{2,3,6–8,10,12} **M_D** was prepared from a PPA containing a sequence of D-amino acids to inhibit cleavage of the substrate by the protease. These two PPAs were synthesized by employing ring-opening metathesis polymerization (ROMP)^{28,29} because ROMP initiators can facilitate the highly efficient graft-through polymerization of peptide-based monomers. Graft-through polymerization of this kind allows for the predictable synthesis of complex block copolymers in a single pot, avoiding the need for unpredictable and often low-yielding post-polymerization modifications with functionalized oligopeptides.^{15,16} The polymerization reactions were terminated using a symmetrical olefinic termination agent consisting of a Boc-protected amino group. Subsequent deprotection and

Received: August 7, 2013

Published: December 5, 2013

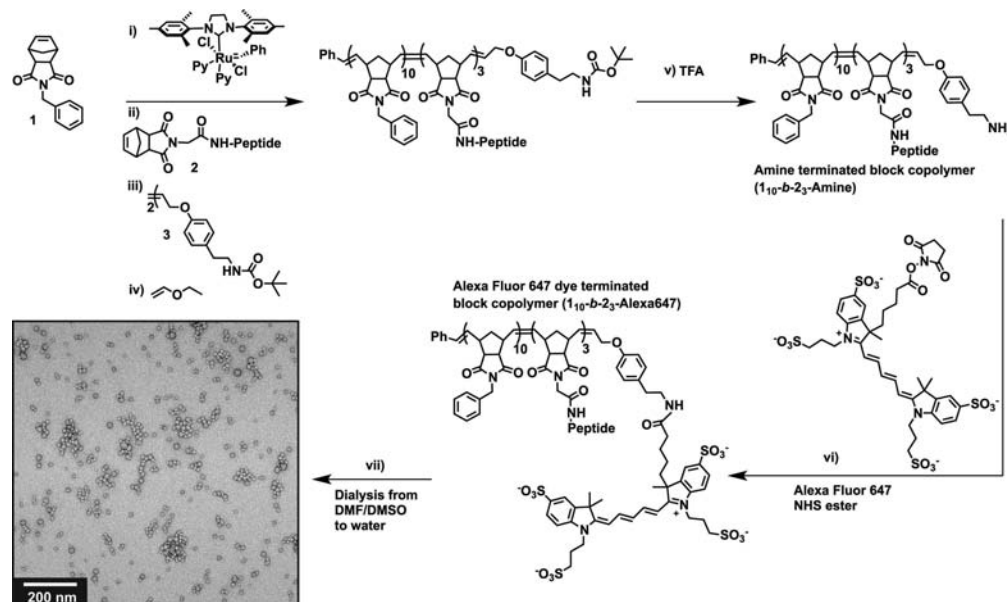


Figure 1. Preparation of enzyme-responsive Alexa Fluor 647-labeled micellar nanoparticles. L-amino acid based norbornyl-peptide substrates were polymerized to generate PPA-L (L-amino acid PPA) for assembly to give micelle, M . D-amino acid based peptides were utilized to generate PPA-D (D-amino acid PPA) for the preparation of nonenzyme responsive control micelle, M_D . Block sizes were determined by SEC-MALS analysis and ^1H NMR spectroscopy. Synthesis: (i) **1** was mixed with Grubbs' third-generation, modified initiator for 30 min, and an aliquot analyzed by SEC-MALS to confirm degree of polymerization. (ii) Peptide monomer was added and stirred for 2 h. Confirmation of 10:3 block copolymer ratio was again determined by SEC-MALS. (iii) The polymer was terminated with amine termination agent for 1 h followed by addition of ethyl vinyl ether (iv) to quench the catalyst. (v) The Boc-protecting group was removed by addition of 90% TFA/DMF for 1.5 h followed by precipitation with ether. (vi) 1.2 equiv of Alexa Fluor 647 NHS ester was reacted with amine terminated polymers for 18 h followed by precipitation with ether. Vacuum dried polymers were then dissolved in 1:1 DMF/DMSO and dialyzed against PBS (pH 7.4) buffered water to generate micellar nanoparticles (M shown in TEM inset). Peptide sequences L-amino acid sequence: GPLGLAGGWGERDGS. D-amino acid sequence: gplglagGWGERDGS (lower case indicates portion of D-amino acids).

reaction with the activated NHS-ester of Alexa Fluor 647 lead to the formation of Near-IR fluorescently tagged PPAs. These are subsequently formulated into 25 nm spherical micelles via dialysis from DMSO/DMF into PBS buffered water over 24 h with three buffer changes.

The enzyme-responsive nature of M and M_D was initially tested *in vitro* by mixing micelles with MMP-9 at 37 °C, followed by TEM analysis (Figure 2S). These experiments confirmed that M and not M_D underwent an accumulation process following cleavage of peptides in the shell of the micelles. These *in vitro* studies were followed by *in vivo* experiments conducted in mouse models inoculated with HT-1080 human cancer cells to generate xenografts known to contain elevated levels of MMPs (Figures 2 and 3S).^{2,3,6–8,10,12} Both M and M_D were intratumorally injected into two different sets of mice and imaged at eight time points: immediately (1 min) following injection, at 1, 3, and 6 h, and at 1, 3, 5, and 7 days. That is, there were eight animals injected at $T = 0$ with M and eight animals injected at $T = 0$ with M_D . Images are shown for each animal at given time points, immediately prior to the animal being sacrificed. These studies clearly reveal the retention of M within tumors and rapid clearance of the D-amino acid control particle, M_D . This is confirmed from the whole mouse scan in live mice (Figures 2 and 3S), *ex vivo* organ analysis (Figure 4S), and *ex vivo* tumor analysis presented with different thresholds (Figures 5S–8S).

To verify that particle activation and subsequent aggregate retention within the MMP-overexpressing HT-1080 tumor tissue^{2,3,6–8,10,12} occurs in conjunction with observable expression of MMP-9, tumor tissue samples were measured via ELISA following imaging analysis (Figure 9S). A time-course study of

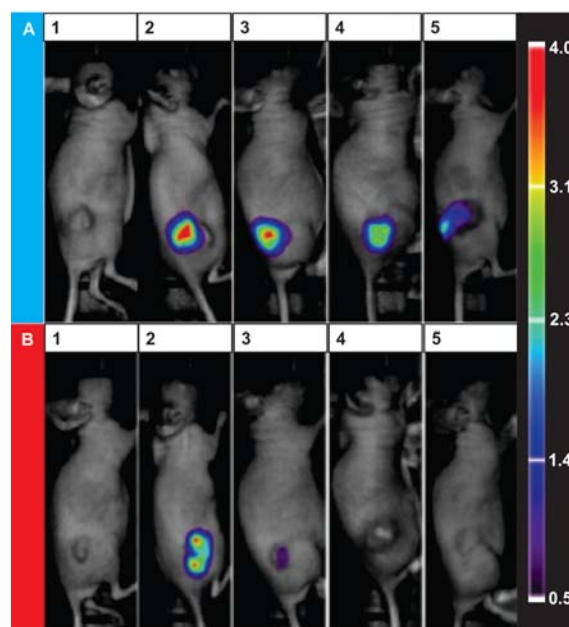


Figure 2. Intratumoral injection to determine relative levels of retention of enzyme-responsive nanoparticles vs control particles with HT-1080 tumors. (A) M injected. (B) M_D injected. (1) Background prior to injection and (2) 1 min, (3) 1 h, (4) 1 day postinjection, and (5) 7 days postinjection. HT-1080 xenograft nude mice with tumor size $\sim 150\text{ mm}^3$ (~ 0.5 nmoles of nanoparticles injected) were utilized for this study. The linear intensity scale bar from 0.5 to 4.0 is given in units of $N_C \times 10^3$, where N_C is number of counts per second per microwatt. The lower threshold is equal to background intensity from control tissue. $\lambda_{\text{ex}} = 635\text{ nm}$ and $\lambda_{\text{em}} = 670\text{ nm}$. See Figure 3S for additional time points.

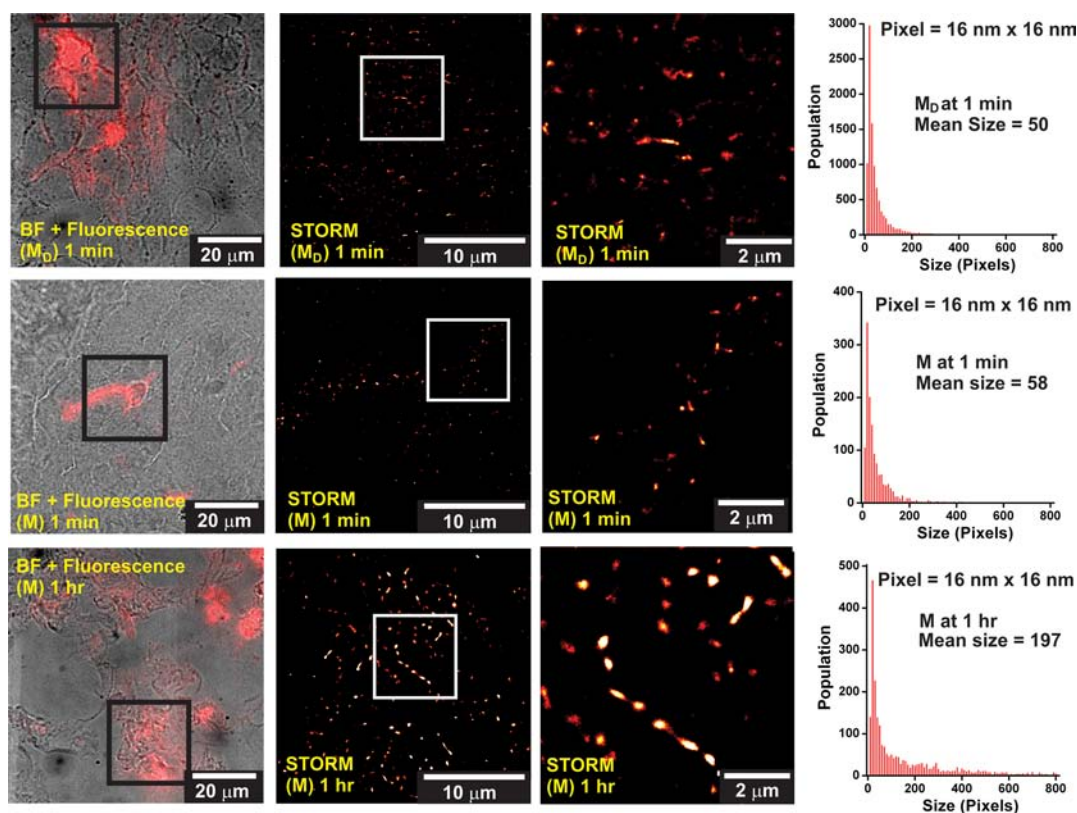


Figure 3. Confocal and super-resolution fluorescence microscopy images of tissue slices from M and M_D intratumorally injected mice. TOP row: M_D injected mice sacrificed at $t = 1$ min postinjection. Middle row: M injected mice sacrificed at $t = 1$ min postinjection. Bottom row: M injected mice sacrificed at $t = 1$ h postinjection. Tumors were removed after sacrificing animals, and tissue slices were prepared for imaging. Left column shows the overlay of bright-field and fluorescence images, where the emission of Alexa Fluor 647-tagged particles is shown in red. The area outlined by the black square was imaged using STORM, as shown in the middle column, where the area outlined by the white square is enlarged in the right column. The sizes of the particles in the STORM images were measured, and the distribution for each condition is shown in the histograms on the right.

the tumor tissues after injection shows constitutive expression of MMP-9. All M and M_D injected tumor tissues possess MMP-9 concentrations with no statistical difference from that of control tumor tissue (no injection) ($p > 0.05$).

We propose the mechanism of retention is the assembly of nanoscale particles into larger, slower clearing particles upon reaction with MMPs. Whole mouse imaging reveals that there is a clear difference in behavior between the unresponsive, D-amino acid containing M_D vs the L-amino acid, responsive M . In support of this interpretation, our previous studies^{1,13} have shown the onset of a FRET signal, unique to the formation of a new assembly in response to the enzymatic cleavage of the substrate, and reorganization of the micelles. However, neither of these studies actually allowed imaging of the assemblies themselves nor were they amenable to whole animal imaging. Therefore, we next analyzed tissue slices taken from mice over a range of time points following injection of both M and M_D . These tissue slices were then analyzed via STORM to determine if retention could be correlated with a concomitant increase in average particle size within the tissue itself (Figure 3). We determined STORM was uniquely capable of imaging a nanoscale size increase within the tissues by breaking the diffraction limit through image reconstruction^{18,22–24} and would reveal information not available in traditional fluorescence microscopy. Prior to STORM analysis, confocal tile scans were first conducted to visualize large areas of tissue (1.06×1.06 mm) to confirm *in vivo* imaging results for the tissue slices to be analyzed at higher magnification (see Figure 10S). These scans revealed

the same pattern of retention of M in tumor tissue for up to a week and clearance of M_D within 1 h of injection. Next, an area was selected for imaging by traditional confocal fluorescence microscopy and overlaid on bright-field images for context (Figure 3, left column). This process was conducted for tissues from M and M_D injected mice (Figure 3; middle and top rows, respectively). Again, these images revealed undetectable signals from M_D injected animals for all samples following the initial injection time point. This confirms successful injection, followed by rapid clearance within 1 h. Therefore, subsequent analyses focused on STORM of M_D injected samples taken immediately following injection (1 min), together with the entire time course of M injected samples (Figure 3). Selected regions (Figure 3: left column, black squares) were subjected to imaging by STORM (Figure 3: middle and right columns).

Quantitative analysis of particle size in each STORM image (Figure 3: histograms) reveals the formation of larger particles at 1 h post injection with M particles. As mentioned earlier, no fluorescence was detected at 1 h post injection with M_D particles (Figure 10S). This is consistent with what can be seen from image analysis of the size of the particles, which reveals an increase in size from initial injection to within 1 h following injection (Figure 3: histograms). The size increase in pixels in M -injected tissue (Figure 3: compare middle and bottom rows) corresponds to an increase from ~ 20 – 100 nm in diameter at 1 min to over 200 nm on average after 1 h. The increased brightness persists and then wanes at 7 days (Figure 10S), again consistent with whole animal imaging, except here, we can

directly observe this as the result of the formation of larger objects, with more dyes per unit area than initially observed immediately following injection. Again, this analysis reveals a similar sized M_D particle at 1 min, and note that this could not be done at 1 h or subsequent time points, because of no detectable fluorescence in the tissue at those later time points. This provides evidence that enzymatically induced aggregation of the materials within the tumor is responsible for their retention for extended periods of time.

In summary, we have utilized Alexa Fluor 647-conjugated peptide polymeric nanoparticles as probes for whole mouse imaging and show extended tumor retention via morphological aggregation in response to MMP enzyme cleavage.¹ Furthermore, we provide compelling evidence that this accumulation process is due to assembly of nanometer particles into larger scale aggregates by employing STORM to study tumor tissue slices *ex vivo*. We observed fluorescent aggregates in targeted tumor tissues within 1 h that were retained for at least 1 week via detailed tissue-slice analysis coupled with whole animal NIR-fluorescence imaging.¹ Most importantly, particles designed to resist reaction with MMPs are cleared from tumor tissues within 1 h as observed in both *in vivo* and *ex vivo* STORM and confocal fluorescence analysis of tissue slices. Together, these studies constitute a previously unexploited coupling of STORM with *in vivo* imaging. We assert that such an approach will be broadly applicable to other targeted materials and is potentially generalizable.

■ ASSOCIATED CONTENT

■ Supporting Information

Experimental details and imaging data. This information is available free of charge via the Internet at <http://pubs.acs.org>.

■ AUTHOR INFORMATION

Corresponding Author

ngianneschi@ucsd.edu

Notes

The authors declare no competing financial interest.

■ ACKNOWLEDGMENTS

The authors acknowledge support for this work from NIH (NIBIB - 1R01EB011633). Furthermore, we thank NIH via a Director's New Innovator Award (1DP2OD008724). N.C.G. acknowledges the Henry & Camille Dreyfus Foundation for a New Faculty Award and the Alfred P. Sloan Foundation for a fellowship. Part of this research was performed using EMSL, a national scientific user facility sponsored by the Department of Energy's Office of Biological and Environmental Research and located at Pacific Northwest National Laboratory.

■ REFERENCES

- (1) Chien, M.-P.; Thompson, M. P.; Barback, C. V.; Ku, T.-H.; Hall, D. J.; Gianneschi, N. C. *Adv. Mater.* **2013**, *25*, 3599.
- (2) Galande, A. K.; Hilderbrand, S. A.; Weissleder, R.; Tung, C.-H. *J. Med. Chem.* **2006**, *49*, 4715.
- (3) Jiang, T.; Olson, E. S.; Nguyen, Q. T.; Roy, M.; Jennings, P. A.; Tsien, R. Y. *Proc. Natl. Acad. Sci. U.S.A.* **2004**, *101*, 17867.
- (4) Kessenbrock, K.; Plaks, V.; Werb, Z. *Cell* **2010**, *141*, 52.
- (5) Olson, E. S.; Jiang, T.; Aguilera, T. A.; Nguyen, Q. T.; Ellies, L. G.; Scadeng, M.; Tsien, R. Y. *Proc. Natl. Acad. Sci. U.S.A.* **2010**, *107*, 4311.
- (6) Querol, M.; Chen, J. W.; Bogdanov, A. A., Jr. *Org. Biomol. Chem.* **2006**, *4*, 1887.

- (7) Scherer, R.; McIntyre, J.; Matrisian, L. *Cancer Metastasis Rev.* **2008**, *27*, 679.
- (8) Simberg, D.; Duza, T.; Park, J. H.; Essler, M.; Pilch, J.; Zhang, L.; Derfus, A. M.; Yang, M.; Hoffman, R. M.; Bhatia, S.; Sailor, M. J.; Ruoslahti, E. *Proc. Natl. Acad. Sci. U.S.A.* **2007**, *104*, 932.
- (9) Tarin, D. *Cancer Microenviron.* **2012**, *5*, 95.
- (10) Tung, C.-H.; Mahmood, U.; Bredow, S.; Weissleder, R. *Cancer Res.* **2000**, *60*, 4953.
- (11) Vartak, D. G.; Gemeinhart, R. A. *J. Drug Targeting* **2007**, *15*, 1.
- (12) von Maltzahn, G.; Harris, T. J.; Park, J.-H.; Min, D.-H.; Schmidt, A. J.; Sailor, M. J.; Bhatia, S. N. *J. Am. Chem. Soc.* **2007**, *129*, 6064.
- (13) Chien, M.-P.; Thompson, M. P.; Lin, E. C.; Gianneschi, N. C. *Chem. Sci.* **2012**, *3*, 2690.
- (14) Ku, T.-H.; Chien, M.-P.; Thompson, M. P.; Sinkovits, R. S.; Olson, N. H.; Baker, T. S.; Gianneschi, N. C. *J. Am. Chem. Soc.* **2011**, *133*, 8392.
- (15) Hahn, M. E.; Randolph, L. M.; Adamiak, L.; Thompson, M. P.; Gianneschi, N. C. *Chem. Commun.* **2013**, *49*, 2873.
- (16) Kammeyer, J. K.; Blum, A. P.; Adamiak, L.; Hahn, M. E.; Gianneschi, N. C. *Polym. Chem.* **2013**, *4*, 3929.
- (17) Bates, M.; Huang, B.; Dempsey, G. T.; Zhuang, X. *Science* **2007**, *317*, 1749.
- (18) Rust, M. J.; Bates, M.; Zhuang, X. *Nat. Meth.* **2006**, *3*, 793.
- (19) van de Linde, S.; Loschberger, A.; Klein, T.; Heidbreder, M.; Wolter, S.; Heilemann, M.; Sauer, M. *Nat. Protoc.* **2011**, *6*, 991.
- (20) Betzig, E.; Patterson, G. H.; Sougrat, R.; Lindwasser, O. W.; Olenych, S.; Bonifacino, J. S.; Davidson, M. W.; Lippincott-Schwartz, J.; Hess, H. F. *Science* **2006**, *313*, 1642.
- (21) Hell, S. W.; Wichmann, J. *Opt. Lett.* **1994**, *19*, 780.
- (22) Dani, A.; Huang, B.; Bergan, J.; Dulac, C.; Zhuang, X. *Neuron* **2010**, *68*, 843.
- (23) Kanchanawong, P.; Shtengel, G.; Pasapera, A. M.; Ramko, E. B.; Davidson, M. W.; Hess, H. F.; Waterman, C. M. *Nature* **2010**, *468*, 580.
- (24) Willig, K. I.; Rizzoli, S. O.; Westphal, V.; Jahn, R.; Hell, S. W. *Nature* **2006**, *440*, 935.
- (25) Tantra, R. K. A. *Nanotoxicology* **2011**, *5*, 381.
- (26) Wang, Z.; Zhang, X.; Huang, P.; Zhao, W.; Liu, D.; Nie, L.; Yue, X.; Wang, S.; Ma, Y.; Kiesewetter, D.; Niu, G.; Chen, X. *Biomaterials* **2013**, *34*, 6194.
- (27) Zhu, M.-Q.; Zhang, G.-F.; Li, C.; Aldred, M. P.; Chang, E.; Drezek, R. A.; Li, A. D. Q. *J. Am. Chem. Soc.* **2010**, *133*, 365.
- (28) Sanford, M. S.; Love, J. A.; Grubbs, R. H. *J. Am. Chem. Soc.* **2001**, *123*, 6543.
- (29) Smith, D.; Pentzer, E. B.; Nguyen, S. T. *Polym. Rev.* **2007**, *47*, 419.